https://doi.org/10.5194/egusphere-2026-4895
Preprint. Discussion started: 19 August 2026

Diabatic contribution to extratropical storm intensification across seasons and its modification under warming

Abel Shibu[1], Henrik Auestad[2], Paulo Ceppi[1], and Tim Woollings[2]
[1]Department of Physics, Imperial College London, London, UK
[2]Atmospheric, Oceanic and Planetary Physics, University of Oxford, Oxford, UK
Correspondence: Abel Shibu (a.shibu24@imperial.ac.uk)

Abstract.

Diabatic processes are important contributors to cyclone intensification. However, precisely quantifying this contribution, and how it may change in a warming world, has remained a challenge. Previous frameworks use simplifying assumptions that constrain their applicability and limit their use to certain parts of the cyclone lifecycle. In this study, we develop a cyclone-centric Potential Vorticity (PV) framework to quantify the contribution from various processes to cyclonic PV intensification and to the maximum relative vorticity that cyclones attain. Applying this framework to cyclones tracked on model runs, we find that the PV intensification in the low-level cyclone is almost entirely associated with the in-situ PV generation from diabatic sources, both for summer and winter. The diabatic contribution to the maximum relative vorticity increases with cyclone strength, from about 35% for a median cyclone to 85% for the strongest cyclones in winter. With warming, low-level winter cyclones show a stronger increase in strength with warming than summer cyclones, which for the strongest cyclones can be attributed to winter cyclones being able to more easily utilise the increase in moisture due to their stronger vertical winds. For the strongest cyclones in both seasons, the vertical wind response with warming decreases the downward penetration of upper-level PV during cyclone intensification, consistent with the low-level cyclones being more diabatically driven. These results point to a "strong gets stronger" response of cyclones with warming, especially in winter, with important implications for extreme weather impacts of global warming.

1 Introduction

Extratropical cyclones (ETCs), hereafter also just referred to as cyclones, are an indispensable part of the mid-latitude general circulation. They play a crucial role in resolving the energy imbalances in the Earth's climate system by transporting heat, moisture and angular momentum polewards (Hartmann, 2007). Features closely associated with these systems are major drivers of midlatitude weather variability (Hawcroft et al., 2012; Konstali et al., 2024), with most of the extreme precipitation and wind events in the midlatitudes also linked with ETCs (Catto and Pfahl, 2013; Owen et al., 2021; Gray et al., 2024). ETCs grow in

https://doi.org/10.5194/egusphere-2026-4895
Preprint. Discussion started: 19 August 2026

regions of high baroclinicity known as the stormtracks (Hoskins and Valdes, 1990; Chang et al., 2002) by the mechanism of baroclinic instability (Eady, 1949; Charney, 1947).

From a Potential Vorticity (PV) framework, cyclone intensification can be conceptualised as consisting of a mutually amplifying, phase locked pair of upper and lower level PV anomalies (Hoskins et al., 1985; Davis and Emanuel, 1991). In the presence of diabatic heating, in particular from the latent heat released in the warm conveyor belt, the strength of this mutual amplification is further increased (Stoelinga, 1996). Consequently, the effect of diabatic processes and their interaction with the adiabatic flow leads to an enhanced cyclone intensification (Kuo et al., 1991; Davis et al., 1993).

PV is a conserved quantity under adiabatic flow, and assuming a set of balance and boundary conditions, the knowledge of the PV field can be inverted to retrieve the wind and geopotential fields. Moreover, the modification of PV in the presence of diabatic processes can also be accounted for via a source term. Naturally, this framework has been used extensively, particularly in previous studies that focused on the role of diabatic heating in cyclone intensification (Büeler and Pfahl, 2017, 2019) and propagation (Tamarin and Kaspi, 2016; Tamarin-Brodsky and Kaspi, 2017).

With an increase in the mean global temperatures, the near-surface moisture availability increases at a rate close to that dictated by the Clausius-Clapeyron equation (Held and Soden, 2006; Schneider et al., 2010), leading to a larger potential for diabatic heating and its consequent effects on the low-level cyclone characteristics and statistics. From channel models, Booth et al. (2013) and Tierney et al. (2018) suggest that with increased moisture availability, the strength of ETCs increases while their size decreases, consistent with Emanuel et al. (1987). However, Tierney et al. (2018) show that the strength of ETCs with increased moisture availability exhibits a non-monotonic behaviour and only increases up to a point, which is also in agreement with Pfahl et al. (2015) who studied cyclones in an idealised general circulation model for a range of climates. Furthermore, Pfahl et al. (2015) highlight that the intensity of the strongest storms continues to increase in warmer models, different from the response of the average storms. Subsequently, Sinclair et al. (2020) used a prescribed-SST full-complexity atmospheric model to show that warming increases the width of the ETC intensity distribution, leading to a "strong get stronger and weak get weaker" response in ETC strength with warming. These studies unveil a complex relationship between moisture availability and the low-level ETC strength, depending on the strength of the ETC group and, to some extent, the model setup.

Given the importance of diabatic processes for ETC intensification, and the largest response to warming expected for the strongest group of cyclones in particular, it is useful to introduce a diagnostic to quantify the role of diabatic processes in cyclone intensification and its change with warming. A diagnostic of the aforementioned nature was proposed by Büeler and Pfahl (2017, 2019). The PV tendency from diabatic processes is estimated by assuming a balance between the diabatic PV generation and the PV advection terms, where PV is assumed to be in a steady state. The PV contributions from the diabatic processes are then averaged over an 'effective' area around the cyclone, determined using a threshold on the vertical wind field. Correctly determining this 'effective' area to average over is important given the tilted vertical structure of cyclones, and simply considering a fixed radius around the low-level cyclone will fail to capture the full cyclone (Čampa and Wernli, 2012). Although this method is quite successful at reproducing the low-level PV field, even for individual cyclones, this methodology does not fully solve for the vertical tilt of cyclones and the assumption of steady state PV limits the use of this methodology to regions where diabatic PV generation is a dominant term, and to timesteps where the cyclone does not intensify much.

https://doi.org/10.5194/egusphere-2026-4895
Preprint. Discussion started: 19 August 2026

The aim of this study is to first introduce a new diagnostic suitable for this purpose that addresses some of the aforementioned issues. We do this by using the full three-dimensional Ertel PV field, which allows us to capture and account for the vertical structure of ETCs across time and enables us to compute PV contributions from both diabatic and adiabatic processes. After we describe and validate this framework, we use it to quantify the contributions from diabatic processes to low-level cyclonic PV and maximum vorticity of cyclones of different strengths, taken from a set of climate model simulations and a reanalysis dataset. Finally, we investigate how these contributions change with warming, with a particular focus on the strongest ETCs.

2 Data and setup

We use data from previous studies (Auestad et al., 2025, 2026) for which simulations with the Community Atmosphere Model 4.0 (CAM4) were performed. The model was run in two configurations — 'control' and 'p4K'. For the control run, CAM4 is run with topography and seasonally varying climatological sea surface temperature (SST) from the period 1995–2005 (Hurrell et al., 2008). The p4K run has the same configuration as control, except with SST increased uniformly by 4 K. Both configurations are run for 50 years (excluding a spinup period of 1 year), with a grid spacing of 0.9 degrees meridionally, 1.25 degrees zonally and 26 vertical levels. We store the model output as six-hourly averages, including temperature tendencies due to latent heating and the total diabatic temperature tendency (from model physics parametrizations).

For each model configuration (control and p4K) and each season (DJF and JJA), we first identify all cyclones in the Southern Hemisphere (SH) that have a lifetime of at least 4 days, have travelled at least 1000 km, lived exclusively outside the tropics (poleward of 30 degrees) and spent at least half of their lifetime in the corresponding season. We identify these cyclones from the relative vorticity field at 850 hPa (spectrally truncated to T42 and wavenumbers less than or equal to 5 removed), using the TRACK algorithm (Hodges, 1994, 1995, 1999). Points are only considered for tracking if the absolute value of the 850 hPa relative vorticity is greater than 10^{-5} s^{-1}. In this study, we restrict our analysis to the SH — this allows us to validate the framework and understand the response of cyclones in a near-zonally symmetric hemisphere before extending it to the Northern Hemisphere. We tracked around 130 cyclones per year in the summer of the control run, and 164 cyclones in winter. For the p4K run, these numbers decreased to 122 and 147 respectively. These trends are in agreement with Priestley et al. (2020) and Priestley and Catto (2022).

Once these cyclones are identified, we centre these cyclones at their points of maximum intensity and truncate each track to only include points 60 hrs before and after the time of maximum intensity. Using the lat-lon position of the tracks, we compute the propagation velocity of the cyclone using a centred differencing scheme (only computed if the cyclone position at –6 hrs and +6 hrs is known). The vorticity, position and velocity of the resultant tracks are then stored. Finally, we sort the cohort of cyclones by their maximum relative vorticity into 20 bins of equal numbers of cyclones.

https://doi.org/10.5194/egusphere-2026-4895
Preprint. Discussion started: 19 August 2026

3 Computing cyclone-centric quantities

Using the truncated cyclone tracks, we compute various quantities of interest for each cyclone around the cyclone centre and across standard pressure levels. These quantities are first computed on the native model grid, and then conservatively interpolated onto a local Cartesian grid centred at the cyclone location that spans a distance of 1680 km in both horizontal directions, with a grid resolution of 40 km x 40 km. A domain of this size is larger than the average cyclone and ensures that we capture most features across cyclones. All quantities are computed at standard pressure levels and 2 days before and after the time of cyclone maximum vorticity.

Ertel PV (Q) is our primary quantity of interest, and is computed following Tamarin and Kaspi (2016), as

$$Q = -g(f\mathbf{k} + \nabla_p \times \mathbf{u}) \cdot \nabla_p \theta, \tag{1}$$

where ∇_p = ($\partial/\partial x$, $\partial/\partial y$, $\partial/\partial p$) is the gradient operator with pressure as the vertical coordinate, $\mathbf{u}$ is the wind, f is the planetary vorticity, g is the acceleration due to gravity and θ is the potential temperature.

We also compute the total Eulerian PV tendency ($\dot{Q}$) as

$$\dot{Q} = -u \cdot \nabla_p Q - g(f\mathbf{k} + \nabla_p \times \mathbf{u}) \cdot \nabla_p \dot{\theta}, \tag{2}$$

where the PV tendency is expressed as the sum of PV advection due to wind and the PV generated from diabatic sources. Here, we neglect the explicit contributions of friction to PV. $\dot{\theta}$ is computed from the total diabatic temperature tendencies which are directly outputted by the model.

For later use, we also compute a modified version of Ertel PV, Q_{rel}, with the planetary vorticity term removed as

$$Q_{\mathrm{rel}} = -g(\nabla_p \times \mathbf{u}) \cdot \nabla_p \theta. \tag{3}$$

3.1 Diabatic PV tendency

In general, there are two different methods used for the computation of the diabatic contribution to PV. Some studies compute it as the PV induced as a direct result of the change in stability induced by diabatic tendencies (Tamarin and Kaspi, 2016; Büeler and Pfahl, 2017). We hereafter refer to this as the 'simple diabatic tendency', formulated as

$$\dot{Q}_{\mathrm{simple}} = -g(f\mathbf{k} + \nabla_p \times \mathbf{u}) \cdot \nabla_p \dot{\theta} = Q \frac{\partial \dot{\theta}}{\partial p} \left(\frac{\partial \theta}{\partial p} \right)^{-1}. \tag{4}$$

Hoskins et al. (1985) and Kohl and O'Gorman (2022) argue that in addition to the direct PV induced by the stability changes, the first-order vertical advection response to the diabatic forcing should also be accounted for and added in. We henceforth refer to this as the 'generalised diabatic tendency', which can be formulated as

$$\dot{Q}_{\mathrm{general}} = Q \frac{\partial \dot{\theta}}{\partial p} \left(\frac{\partial \theta}{\partial p} \right)^{-1} - \dot{\theta} \frac{\partial Q}{\partial p} \left(\frac{\partial \theta}{\partial p} \right)^{-1}. \tag{5}$$

The additional term can be understood as the cross-isobaric ascent induced as a direct result of diabatic tendencies in the framework of isentropic coordinates (Martínez-Alvarado et al., 2016), and its inclusion enables us to better isolate the impacts

https://doi.org/10.5194/egusphere-2026-4895
Preprint. Discussion started: 19 August 2026

of diabatic processes in accordance with the principle of ‘PV impermeability’ (Haynes and McIntyre, 1987). In this study, we compute both the simple diabatic and general diabatic terms and show that the generalized diabatic term is more representative of low-level cyclone intensification and its response to warming.

4 Computing cyclone intensification

With the aim of isolating and computing the PV intensification in cyclones while excluding all tendencies associated with their propagation, we consider the scenario shown in Fig. 1. Here, we show an idealised cyclone and its Eulerian PV tendency at a particular pressure level, with the cyclone propagating towards the right in the plane. Note that this is a snapshot in time, with the x-axis being the horizontal spatial dimension of the cyclone.

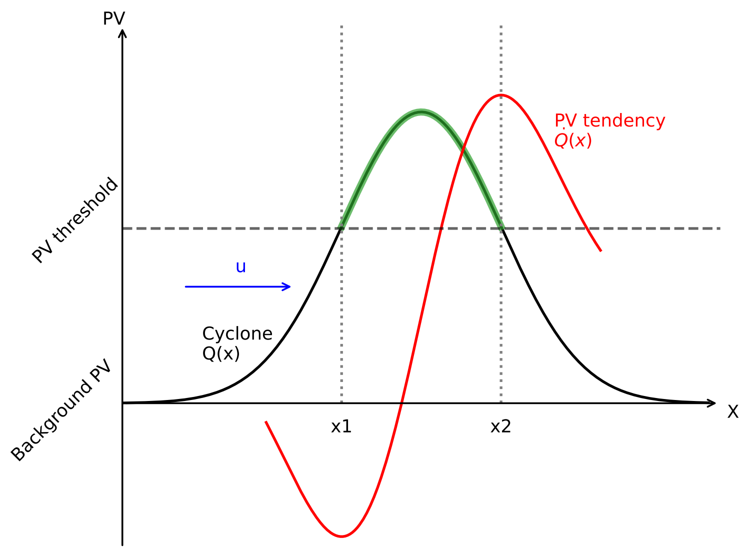

Figure 1. Schematic of an idealised cyclone and the Eulerian PV tendency (shown in red) associated with it. The cyclone is depicted to be intensifying, while at the same time propagating towards the right with velocity u. The green portion indicates the region identified as the cyclone, based on a PV threshold shown by the dashed line, where x_1 and x_2 are the spatial bounds of this region.

We can split the total PV tendency $\dot{Q}(x)$ as

$$\dot{Q}(x) = \mathrm{int}(x) + \mathrm{prop}(x), \tag{6}$$

where int and prop are associated with cyclone intensification and propagation, respectively. Assuming that the instantaneous rate of change of the shape of the cyclone is small, we can replace $\mathrm{prop}(x)$ by $-u\frac{\partial Q}{\partial x}$, where u is the velocity of the cyclone centre. Integrating both sides over x from x_1 to x_2 (see Fig. 1), and dividing by the length $x_2 - x_1$, we obtain the average values

https://doi.org/10.5194/egusphere-2026-4895
Preprint. Discussion started: 19 August 2026

of the tendency terms over the cyclone area as

$$\frac{1}{x_2 - x_1}\int_{x_1}^{x_2} \dot{Q}(x) = \frac{1}{x_2 - x_1}\int_{x_1}^{x_2} \mathrm{int}(x) - \frac{u}{x_2 - x_1}\int_{x_1}^{x_2} \frac{\partial Q}{\partial x}. \tag{7}$$

$\frac{1}{x_2 - x_1}\int_{x_1}^{x_2}$ is an operator that returns the average value between x_1 and x_2. Denoting this average using $\langle\rangle$, integrating the second term on the RHS and rearranging, we get

$$\langle \mathrm{int}(x)\rangle_{[x_1,x_2]} = \langle \dot{Q}(x)\rangle_{[x_1,x_2]} + \frac{u}{x_2 - x_1}(Q(x_2) - Q(x_1)). \tag{8}$$

Equation 8 allows us to compute the intensification of the cyclone as the sum of the average PV tendency in the cyclone area and a term associated with the PV structure of the cyclone. Note that the PV tendency term can be split into individual contributing terms, while the second term on the RHS cannot be. This motivates us to minimise this term, which can be done by selecting x_1, x_2 such that $Q(x_1) = Q(x_2)$. We do this by simply selecting the cyclone region using a threshold on PV (as shown in Fig. 1).

In the next section, we extend this approach to compute the PV intensification for the average cyclone in our strength groups.

5 Cyclone mask

To compute the PV intensification for an average cyclone, we need to compute the bounds of the cyclone using a PV threshold similar to in Fig. 1. We do this by utilising percentile thresholds on the horizontal field at each height level and time. The procedure is as follows:

1. First, we filter out PV data at points where individual cyclones are polewards of 70 degrees and set them to missing (NaN) values. This is to avoid the artifacts from cyclones interacting with the prescribed ice regions in the model.

2. As PV increases polewards, simply selecting points based on a PV threshold would select some regions at the poleward edge of the box not associated with the cyclone. To prevent this, we compute a low threshold (60th percentile) on the quantity Q_{rel} (defined in section 1.2) at every pressure level and time, across individual cyclones. We set the PV at points that do not meet this threshold to zero. Q_{rel} is the ideal quantity for this purpose because it is similar to PV, except without the Coriolis term. Filtering using a low threshold on Q_{rel} ensures that most of the regions of high PV are retained, while excluding the term that increases most strongly polewards.

3. The resultant, filtered PV field is used to compute the composite PV field for the cyclone group. However, before we compute the PV composite, we normalise the PV field of each cyclone at each level and time by the strength of the field — defined as the average PV in the region that exceeds the 95th percentile of PV. This step ensures that the composite is representative of all cyclones and not just the strongest ones. For timesteps where the data does not exist (outside the lifetime of a particular cyclone), the corresponding values are treated as missing (NaN) values for the compositing.

https://doi.org/10.5194/egusphere-2026-4895
Preprint. Discussion started: 19 August 2026

4. Finally, we set a PV threshold of the 95th percentile (for each level and timestep) on the composite normalised PV obtained from (1–3) to get the composite cyclone mask for the group. A threshold of the 95th percentile (computed over a square region of side length 1680 km) results in an area of size similar to that used by previous studies (Büeler and Pfahl, 2017; Čampa and Wernli, 2012), and ensures that we capture most of the cyclone features associated with diabatic heating. Also, as we have a large number of cyclones in each group, no smoothening of the PV field is required.

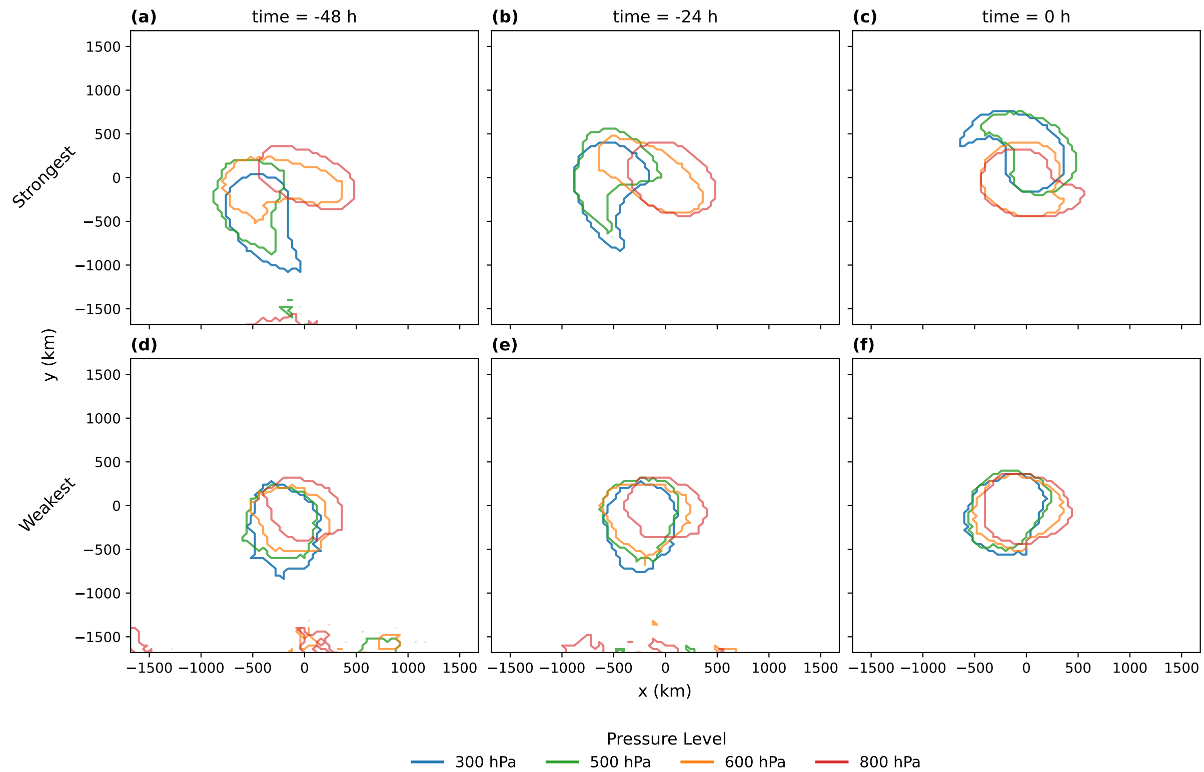

Figure 2. Cyclone masks for the strongest (a–c) and weakest (d–f) 5 percent of SH winter cyclones in the control run at pressure levels of 300, 500, 600 and 800 hPa and their evolution across time. Shown are profiles for 48 hours before, 24 hours before and at maximum relative vorticity.

Steps (1–3) help to obtain the cleanest possible cyclone mask, but the results remain fairly similar even if they are skipped (not shown). The normalisation in step 3 can be skipped if the cyclones are of similar strengths. We compute the cyclone mask for cyclones in each strength group — Fig. 2 shows the final cyclone masks obtained by this method for the strongest and weakest winter cyclone groups in the control run. In general agreement with Köhler and Sinclair (2026), the cyclone masks capture the general features of strong and weak extratropical cyclones, like the tilt with height and its evolution across time. The quasi-vertical structure of strong ETCs up to around 600 hPa (Čampa and Wernli, 2012), with a rapid increase in tilt higher up also emerges naturally.

https://doi.org/10.5194/egusphere-2026-4895
Preprint. Discussion started: 19 August 2026

Note that on the local Cartesian coordinate system we use, selecting regions based on percentile thresholds has the benefit of maintaining a constant area. This allows for direct comparison between different cyclone groups, and across time. Also, while we have not explicitly forced the points in the cyclone mask to be connected to each other, this feature emerges intrinsically from the methodology. Although this leads to some isolated regions being identified in some timesteps (as seen in Fig. 2), they are sufficiently small that their effect on the results can be neglected.

6 Composite cyclone intensification

Utilising the cyclone masks described in the previous section and reformulating Eq. 8, we can compute the PV intensification across time and height of the average cyclone. The 1D average in Eq. 8 is generalised to be the average over the cyclone mask at each level and time. The first term $\dot{Q}$ is computed using the formulation in section 3. Given that we have used a PV threshold to compute the cyclone mask, the second term is minimised. However, a term of this form should still be computed and added in as a residual to get the best estimate for the cyclone PV intensification.

This residual is computed in two parts. The first part is a term that captures the PV advection due to the propagation of the cyclone as a whole. As the cyclone tracking is done at 850 hPa, this propagation with velocity u_c is from the perspective of the cyclone centre at 850 hPa. This can be seen in Fig. 2, with the lowest level cyclone appearing fixed at the centre of the domain. However, the cyclone region at higher levels moves around relative to the domain. This motion of the cyclone region with respect to the domain also needs to be added in to the residual. The velocity of the cyclone mask with respect to the domain u_cl is computed by tracking the location of the centroid of the cyclone region at each level across time with respect to the domain. A term similar to the first part is then computed for each level and time.

Overall, the total PV intensification of the cyclone at each level and time can be computed as

$$\langle \mathrm{int}(p,t)\rangle_A = \langle \dot{Q}(p,t)\rangle_A + \langle (u_\mathrm{c}(t) + u_\mathrm{cl}(p,t)) \cdot \nabla_p Q(p,t)\rangle_A, \tag{9}$$

where A is the area identified by the cyclone mask and p is the pressure level. The first term on the RHS is as defined in section 3, and can be split further into contributing terms. The second term is the propagation residual, and cannot be split further. Given that all the cyclones in a group share the same mask, the order that the averages are computed does not matter (averaging across cyclones and averaging in the mask). Note that the PV intensification at timesteps where any particular cyclone does not exist is set to zero, and to missing (NaN) values at timesteps where cyclones are poleward of 70 degrees. This ensures that the PV intensification is consistent from the perspective of the average cyclone, and avoids amplifying the signal at timesteps with fewer cyclones.

The total PV intensification across height and time can be shown using a Hovmöller plot. Figures 3a and 4a show these plots for the strongest winter and summer cyclone groups in the control run, respectively. Note that as the values of PV are negative in the SH, the colourbars are inverted in these plots to order values from the most positive (blue) to the most negative (red). We see that these plots capture the low-level cyclone intensification leading up to maximum vorticity, and the PV decay after. The low-level PV tendencies are accompanied by tendencies of the same sign in the upper troposphere, reminiscent of

https://doi.org/10.5194/egusphere-2026-4895
Preprint. Discussion started: 19 August 2026

the concept of ETCs being a mutually amplifying pair of PV anomalies (Davis and Emanuel, 1991), although we use the full PV field instead of PV anomalies. Between summer and winter, the strongest summer cyclones have larger values of PV and PV tendencies despite winter cyclones being stronger in terms of relative vorticity. This seasonal difference was also noted by Čampa and Wernli (2012), and may be attributed to summer cyclones being located at a higher latitude in general and having a more stratified temperature profile in comparison to winter cyclones. The low-level summer cyclones also seem to intensify bottom-up, in comparison to the low-level winter cyclones. This is consistent with a larger diabatic contribution to PV (Köhler and Sinclair, 2026) in summer relative to winter.

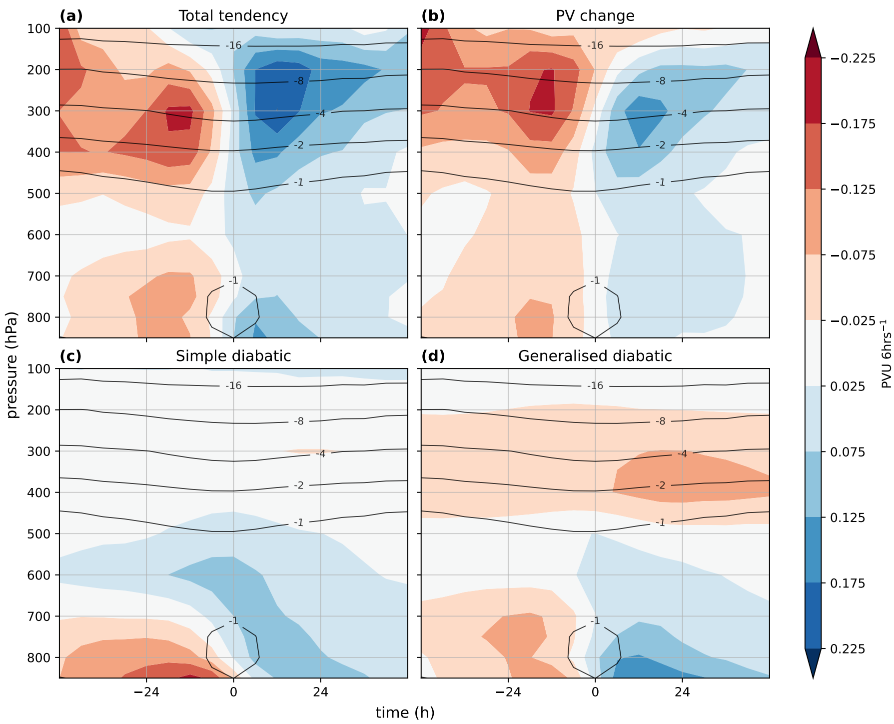

Figure 3. Hovmöller plots for the strongest winter cyclones in the control run. As PV values are negative for SH cyclones, the colourbar is inverted and negative PV tendencies (red) correspond cyclone intensification. Plots for (a) The total PV intensification (as computed in Eq. 9). (b) $\frac{d\langle Q\rangle}{dt}$, which should be similar to the total intensification. (c) The diabatic term (Eq. 4). (d) The generalised diabatic term (Eq. 5). The contour lines in all plots show the Hovmöller pattern for PV across time.

Figures 3c and 4c show the Hovmöller plots associated with the simple diabatic term (Eq. 4). We see that the simple diabatic term generates cyclonic PV in the lower troposphere during the intensification phase, accompanied by anticyclonic PV generation above, which is expected from the opposite signs of stability changes above and below the location of diabatic heating (Tamarin and Kaspi, 2016). The PV generation also occurs at a higher altitude in summer in comparison to winter, and is consistent with latent heat release occurring higher up in a warmer environment (Tierney et al., 2018).

https://doi.org/10.5194/egusphere-2026-4895
Preprint. Discussion started: 19 August 2026

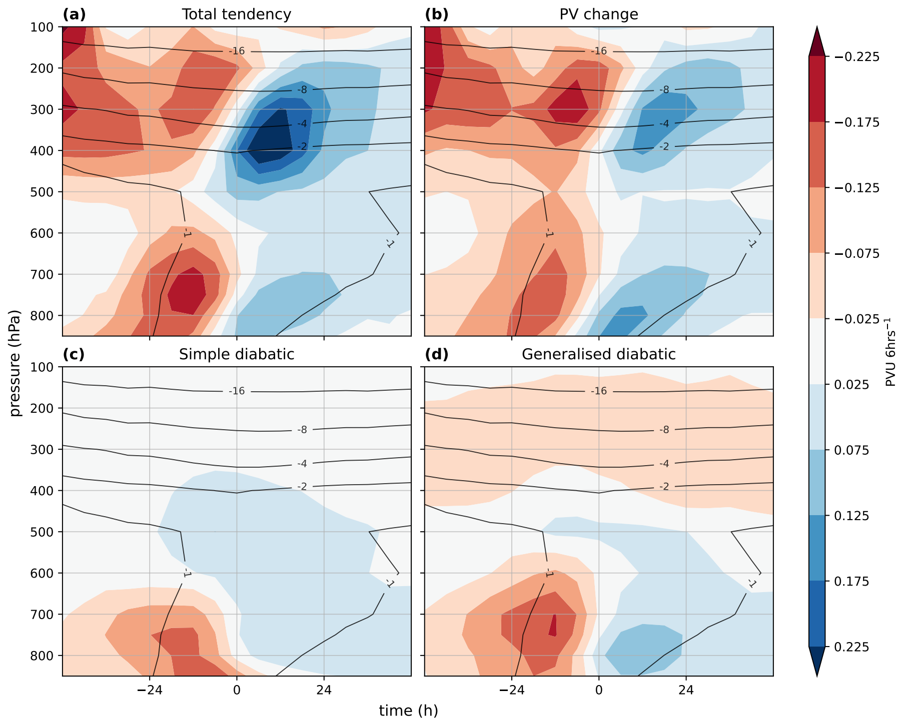

Figure 4. Same as Fig. 3, but for the strongest summer cyclones in the control run.

We then compare the simple diabatic term to the generalised diabatic term (Eq. 5). We see that the generalised diabatic term (panel d in Figs. 3 and 4) is a much better representation of the total tendency patterns (panel a) at the lower troposphere (below 500 hPa in summer and 600 hPa in winter), both in its magnitude and pattern. The vertical advection during the intensification phase neutralises the overlying anticyclonic (positive) PV generation. The anticyclonic PV generation is now confined to the decay phase, where the vertical response leads to a further increase in the cyclone decay at the lower troposphere. The PV generation in the upper troposphere is a direct result of longwave radiative cooling close to these levels (not shown, but consistent with Chagnon and Gray, 2015), which induces subsidence and vertical advection of air with high cyclonic PV. Given that the generalised PV term better isolates the effects of diabatic PV generation (Hoskins et al., 1985) and matches the pattern of the total PV tendency, we adopt this form for the rest of this study. Henceforth, the generalised diabatic term $\dot{Q}_{\mathrm{generalized}}$ is simply called the diabatic term $\dot{Q}_{\mathrm{diab}}$.

6.1 Method validation

To validate our methodology, we compute the average PV, $\langle Q(p,t)\rangle$, for the strongest winter and summer cyclone groups using the cyclone mask at each level and from –48 h to 48 h. We can then estimate the rate of change of $\langle Q\rangle$ with time as $\frac{d\langle Q\rangle}{dt}$, which should be similar to the total PV intensification computed using Eq. 9. Here, a centred differencing scheme is used except at -48

https://doi.org/10.5194/egusphere-2026-4895
Preprint. Discussion started: 19 August 2026

h and 48 h, where forward and backward differencing schemes are used. From panel (b) in Figs. 3 and 4, we see the Hovmöller plots for the PV change $\frac{d\langle Q\rangle}{dt}$ matches well with that of total intensification, showing that the PV tendencies combined with the cyclone masks capture the changes in PV reasonably well. The mismatch between the exact patterns of PV change and the total tendency can be attributed to the quantities themselves being slightly different — the tendency is instantaneous, while the PV change is the rate of change of PV averaged over 12 hours around each point in time.

As an additional test for the methodology, we repeat the analysis for the strongest winter and summer cyclones tracked on 10 years of data (1995–2004) from MERRA2 (Global Modeling And Assimilation Office and Pawson, 2015a, b). The resultant Hovmöller plots (Fig. A1) show patterns that are broadly consistent with the CESM CAM4 control run, indicating that the methodology is robust.

7 Diabatic contribution to low-level PV

We now focus on the low-level cyclone and the diabatic contribution to PV at these levels. We define the low-level cyclone to be between 850 hPa and 700 hPa, both in summer and winter. This helps us keep the methodology consistent, remain close to 850 hPa where tracking was performed and avoid the boundary layer, where friction and boundary layer processes might have a significant effect on cyclone strength. This choice is also partially motivated by the vorticity at the time of cyclone maximum averaged in the cyclone mask between these levels being close to the maximum vorticities obtained from tracking across cyclone strength classes (not shown).

The contribution to low-level PV is computed as the mass-weighted average of the PV tendencies between 850 hPa and 700 hPa. The total PV generated is estimated by integrating the PV intensification computed in Eq. 9 over the two days preceding cyclone maximum intensity. As the tendencies are already computed in the units of PVU (6 hrs)$^{-1}$ (See Figs. 3, 4), we add up the six-hourly average PV tendencies up to cyclone maximum. The total diabatic contribution is calculated as the generalised diabatic term (Eq. 5) in a manner similar to the total PV generation. The difference between the total and the diabatic PV generated is then called the ‘adiabatic’. Hence, the ‘adiabatic’ contains PV contributions from the horizontal advection of PV into the cyclone area and the vertical advection of PV that is not associated with the diabatic processes (see Eq. 5). Figure 5 shows how the diabatic and adiabatic contributions add up to the total PV generated up to cyclone maximum intensity for the different strength groups. To validate this result, we also plot the actual change in PV over the two days preceding cyclone maximum. We see that in all considered cases (for both seasons, climates and across the strength groups), the total PV generated up to cyclone maximum can be attributed to diabatic sources, while the adiabatic contribution is small and fluctuates around zero. Moreover, the total contributions are in good agreement with the actual changes in PV. While the tendencies deviate slightly from the actual PV changes especially for the strongest cyclones, this is reasonable given the six-hourly resolution of the data we used and the approximate nature of the comparison itself. These results were also replicated with reasonable agreement for cyclones in MERRA2 data and are shown in Fig. A2.

The right-most column in Fig. 5 also shows the difference between p4K and control runs. We see that there is an overall increase in PV generation with warming in winter, which can be broadly attributed to an increase in the diabatic contribution.

https://doi.org/10.5194/egusphere-2026-4895
Preprint. Discussion started: 19 August 2026

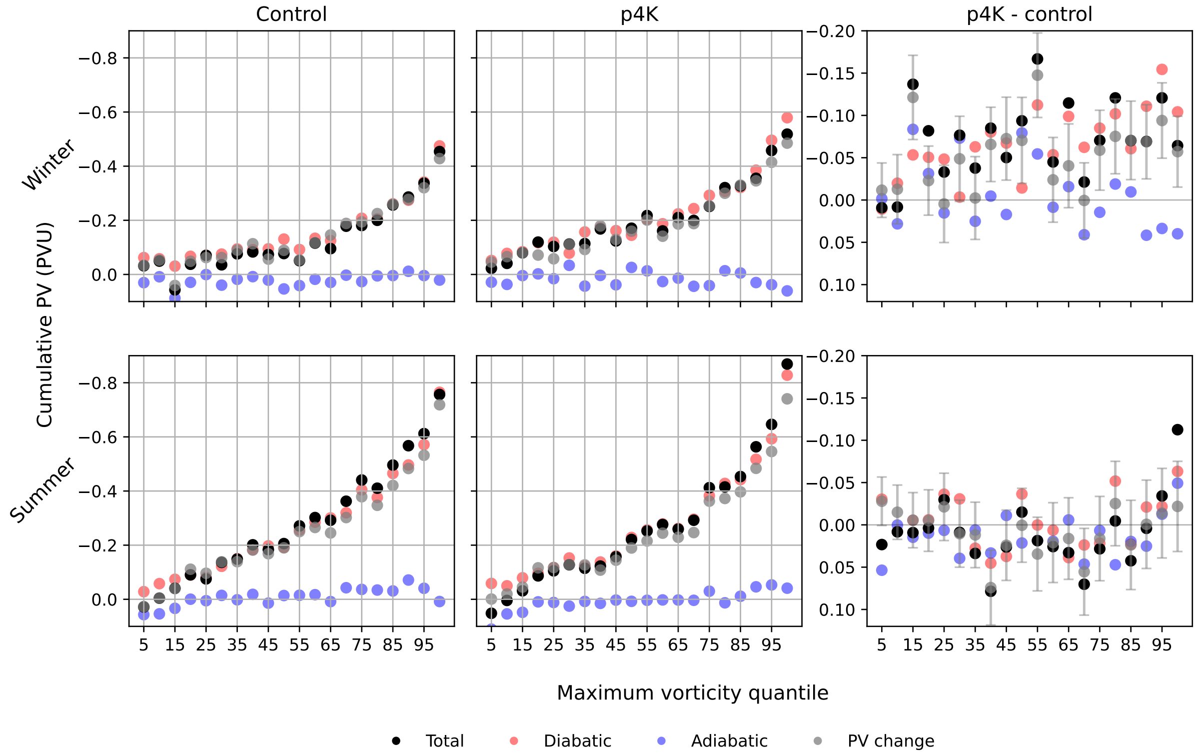

Figure 5. The total PV generated (computed using Eq. 9) in the low-level (850–700 hPa) cyclones of different strength groups during the two days preceding cyclone maximum vorticity. The plots show contributions from the diabatic and adiabatic terms, and also the actual change in PV over the two days preceding cyclone maximum. The right-most column shows the difference between p4K and control, where the error bars show the 95% confidence interval of the modification of the mean PV change.

In contrast, the PV generation in summer decreases slightly across most of the cyclone strength range, except for the strongest and weakest cyclones, where we have little confidence in the sign of the change. The response of cyclones to warming is clearly dependent on the strength class of the cyclone, with the response of the strongest cyclones being quite different from that of the average cyclone.

8 Diabatic contribution to low-level maximum relative vorticity

Although PV generation following cyclones is helpful for understanding their lifecycle, it does not fully explain the strengthening of the cyclones in terms of their low-level maximum relative vorticity. In this section, we shift our focus from PV onto relative vorticity as a measure of cyclone strength and estimate the contribution of different processes to the maximum relative vorticity across the cyclone strength groups. This is achieved by relating the maximum relative vorticity to the PV attained by the cyclones at this time. We follow the group of cyclones during the two days preceding the time of maximum vorticity

https://doi.org/10.5194/egusphere-2026-4895
Preprint. Discussion started: 19 August 2026

and keep track of the amount of PV generated within the composite low-level cyclone in this time frame. Again, we average between 700 hPa and 850 hPa. The final PV attained by the cyclone can then be expressed in terms of the initial PV and the amount of PV generated as

$$Q_{\mathrm{max}} = Q_{\mathrm{i}} + \int_{-2\ \mathrm{days}}^{t_{\mathrm{max}}} \dot{Q}\, dt, \tag{10}$$

where 'max' represents the time of maximum vorticity, and 'i' denotes the initial state two days prior. We split $\dot{Q}$ into the diabatic and adiabatic components and write Q_{max} as $-g(f_{\mathrm{max}} + \xi_{\mathrm{max}})\frac{\partial \theta}{\partial p}$, approximating it to only its vertical component to obtain

$$\xi_{\mathrm{max}} = \frac{1}{-g\frac{\partial \theta_{\mathrm{max}}}{\partial p}}\left(\int_{\mathrm{i}}^{t_{\mathrm{max}}} \dot{Q}_{\mathrm{diab}}\, dt\right) + \frac{1}{-g\frac{\partial \theta_{\mathrm{max}}}{\partial p}}\left(\int_{\mathrm{i}}^{t_{\mathrm{max}}} \dot{Q}_{\mathrm{res}}\, dt\right) + \frac{Q_{\mathrm{i}}}{-g\frac{\partial \theta_{\mathrm{max}}}{\partial p}} - f_{\mathrm{max}}, \tag{11}$$

where ξ is the relative vorticity, θ is the potential temperature, f is the Coriolis parameter and g is the acceleration due to gravity. The first term on the RHS is the contribution of the diabatic term to the maximum vorticity, and is just the diabatic contribution to PV divided by a factor of the low-level static stability at the time of maximum vorticity. The quantities in the numerator and denominator are averaged across cyclones and height levels before the division is computed. The other terms on the RHS combine to be the 'other processes'. From the previous section, we know that the adiabatic term (second term on the RHS) is small. Hence, the terms that contribute most to the other processes are the other two terms — the initial PV (Q_{i}) scaled by the inverse of the low-level atmospheric stability, and the Coriolis parameter at the final location. The first of these terms (third term on the RHS) signifies that the vorticity at the final location can be increased by increasing the distance between isentropes (same as decreasing atmospheric stability). The other term (fourth term on the RHS) reveals the loss/gain of cyclonic vorticity that occurs when a cyclone propagates poleward/equatorward.

Figure 6 stacks the contributions from the diabatic term and the other processes to predict the maximum vorticity of the different cyclone strength classes. The maximum vorticity predicted by this method matches the average maximum vorticity at 850 hPa of the tracked cyclones across strength groups. The approximation that Q_{max} can be attributed entirely to the vertical component of vorticity is inaccurate — there is a significant amount of vorticity in the horizontal directions that contributes negatively to the full Ertel PV. This means that our assumption underestimated the maximum cyclone vorticity. We can correct for this by adding in an extra 'full PV correction' term, computed as the sum of the horizontal components of PV at the time of maximum cyclone strength divided by the static stability (see the appendix for a full derivation). From Fig. 6, the contributions from this term are seasonally different, with its magnitude being systematically stronger in winter than in summer. The other processes have the largest contribution to vorticity for the weakest cyclones, and decreases as we move to stronger cyclones. This pattern of vorticity contribution from the other processes explains how the strength of the cyclones can increase even without much increased PV generation from the diabatic term. This analysis was also performed for cyclones in MERRA2 data, the results of which are shown in Fig. A2. Although predictability of cyclone strength is retained, the seeming underestimation of diabatic processes leads to lower predicted cyclone strengths in reanalysis, especially in winter.

https://doi.org/10.5194/egusphere-2026-4895
Preprint. Discussion started: 19 August 2026

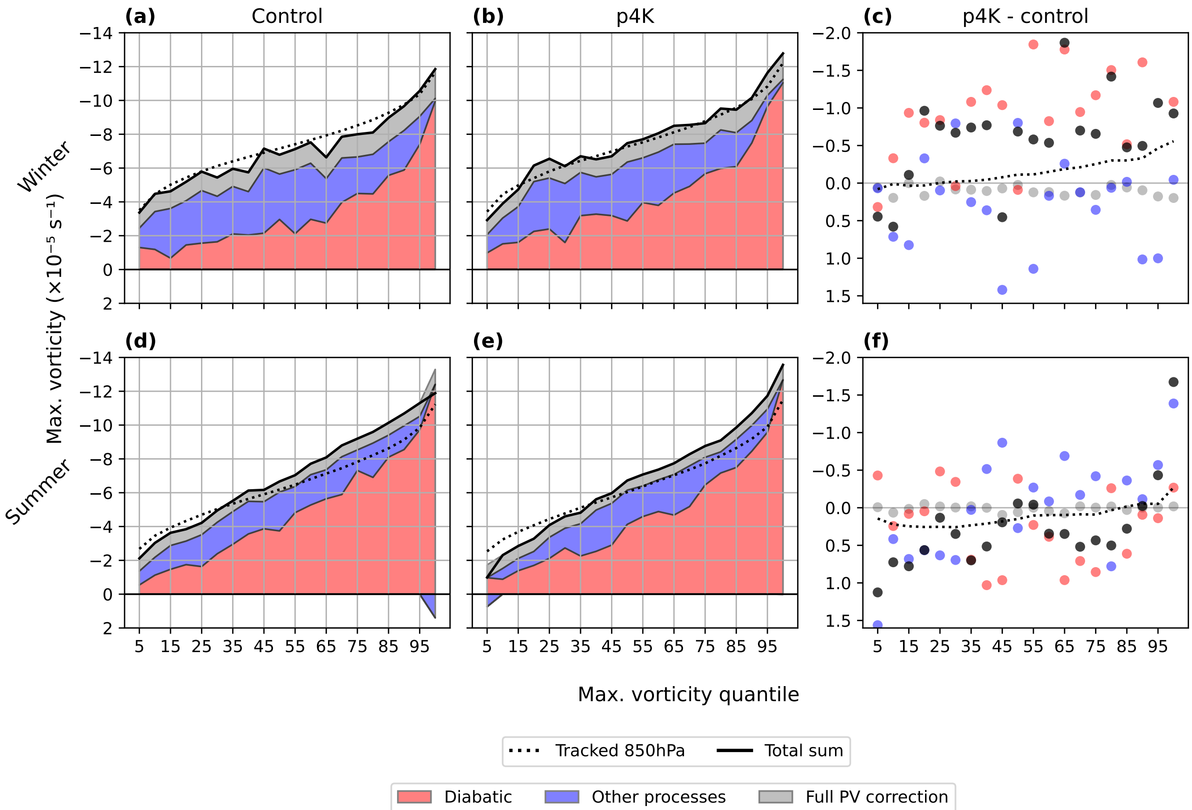

Figure 6. Contributions from the different processes to the total maximum vorticity of the average cyclone across strength classes. The contributions add up to the solid line, which matches the average maximum vorticity of the tracked cyclones across strength groups, shown by the dotted line. The right-most column shows the difference between p4K and control; differences in contributions are not stacked in this case.

From Fig. 6, we see that as we move from weaker to stronger cyclones, the maximum vorticity is increasingly diabatically produced. The diabatic contribution to the maximum vorticity of the median winter cyclone is around 35%, while it is about 85% for the strongest cyclones. Hence, a large part of the vorticity of the strongest cyclones across seasons and model runs can be attributed almost entirely to the low-level PV generated by the diabatic term. The right-most column of Fig. 6 shows the differences in contributions to maximum vorticity between the p4K and control runs. These plots, although noisy, look similar to the rightmost panel of Fig. 5 with an increase in the diabatic contribution across cyclone strength groups in winter and only for the strongest cyclones in summer. The full PV correction term does not change much with warming. For the strongest cyclones in both summer and winter, the increase in maximum vorticity is closest to the increase in diabatic contribution.

The decrease in contribution from the other processes with cyclone strength is explained by the increase in negative contributions from the $f_{\max}$ term due to an enhanced poleward propagation of stronger cyclones during the two days preceding cyclone maximum (panel b in Fig. 7). Cyclones drifting polewards find themselves in an environment of larger cyclonic PV,

https://doi.org/10.5194/egusphere-2026-4895
Preprint. Discussion started: 19 August 2026

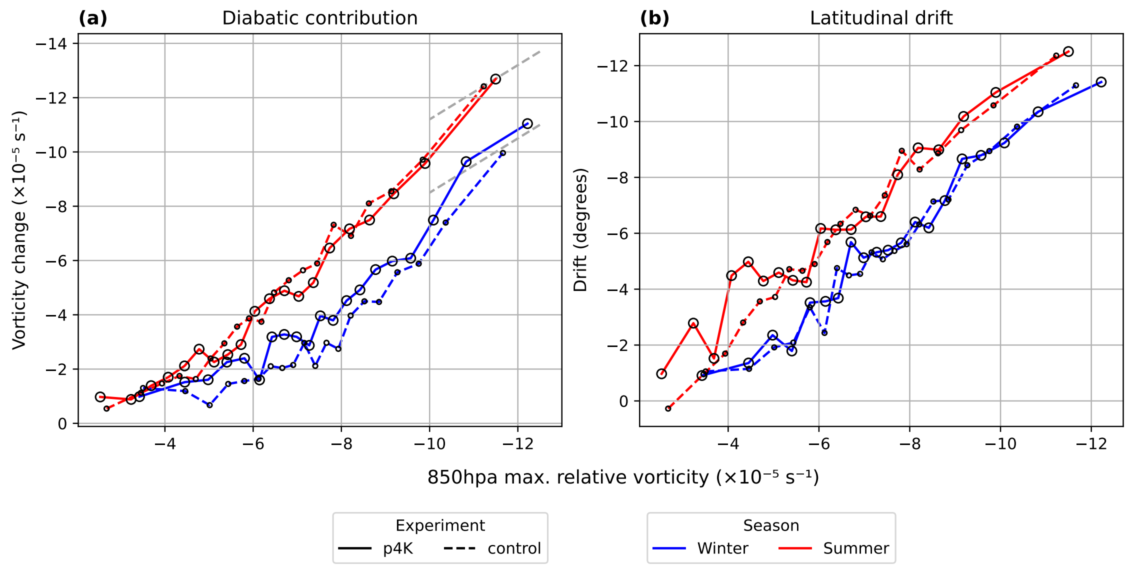

Figure 7. (a) Diabatic contribution to maximum vorticity plotted against maximum vorticity. The grey dashed lines are parallel to the 1:1 line. (b) Same, but for the latitudinal drift.

which leads to a decrease in the magnitude of relative vorticity. Within each season, we see that cyclones of equal strengths drift polewards by similar amounts. However, cyclones in summer systematically drift further polewards than cyclones of equal strengths in winter (See panel b of Fig. 7), although the exact reasons for this are unclear.

It is also interesting to compare the diabatic contributions to cyclones of equal strengths (in terms of maximum relative vorticity) across seasons and examine how it changes with warming. To check this, in panel (a) of Fig. 7, we have plotted the diabatic contribution to the maximum vorticity of the cyclone strength groups against their maximum vorticities. For the summer cyclones, with warming, the lines are essentially overlapping, with the diabatic contribution to cyclones of equal strength remaining unchanged. In winter however, we see a small but systematic increase in the diabatic contribution to equal-strength cyclones. For the strongest cyclones in both seasons, the increase in maximum vorticity is accompanied by an almost equal increase in the diabatic contribution, which is consistent with our findings so far.

9 Changes in the strongest cyclones

From the previous sections, we know that the response to warming is largest for the strongest cyclone groups in both seasons. The fact that the strongest cyclones are also the most impactful further motivates us to understand how these cyclones in particular are modified under warming.

First, we consider how the PV generation from the generalised diabatic term changes with warming. Panels (a) and (c) of Fig. 8 show the difference Hovmöller plots (p4K minus control) for this term for winter and summer, respectively. With warming,

https://doi.org/10.5194/egusphere-2026-4895
Preprint. Discussion started: 19 August 2026

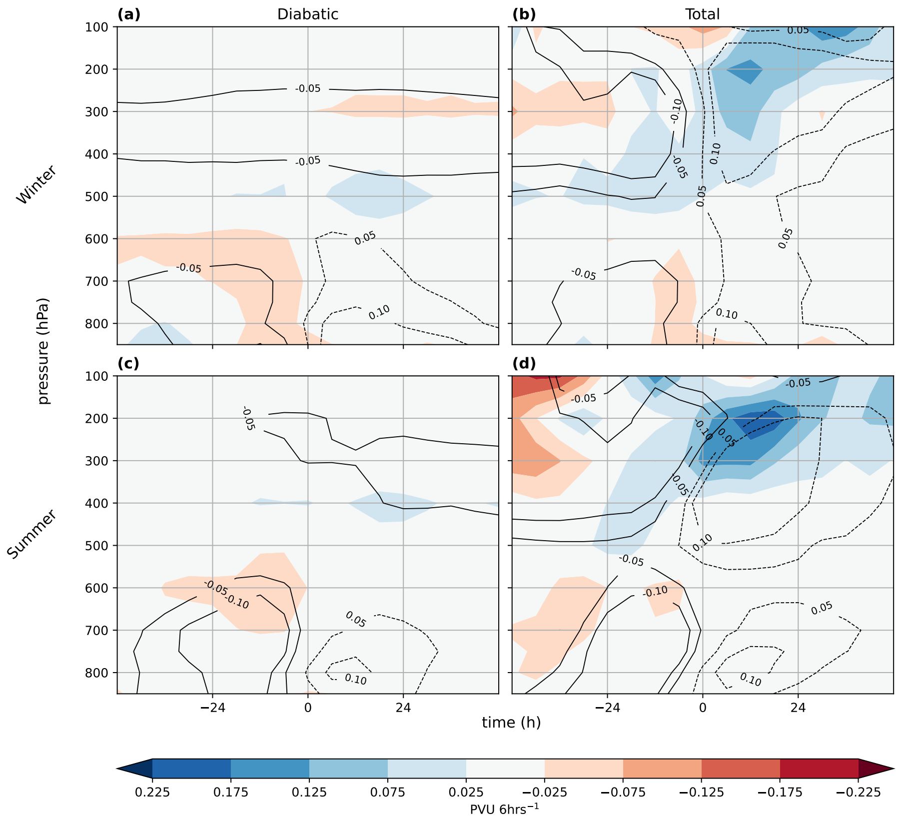

Figure 8. Difference Hovmöller plots for the generalised diabatic term and the total PV intensification between the control and p4K cyclones for the strongest winter (panels a and b) and summer (panels c and d) cyclones. The values of these quantities in the control run are overlaid as contours.

there is an increase in PV generation at the upward flank of the existing pattern for both summer and winter. However, the winter cyclones also show some additional increase at the lowest levels close to the time of cyclone maximum, resulting in a larger low-level diabatic PV response in winter (consistent with Fig. 5). We see that at the lower levels (700–850 hPa) and during cyclone intensification, the difference in the generalised diabatic term resembles the patterns of change in the total intensification (panels b and d) with a stronger response in winter. At the higher levels (starting from 300 hPa) from the time of cyclone maximum, a pattern of anomalous PV decay is also seen. The diabatic temperature tendencies in the lower troposphere above the boundary layer are dominated by latent heating (see Fig. B1 for a comparison of the PV tendency patterns obtained from the total temperature tendency and from only latent heating). Therefore, the increase in the low-level PV tendency with warming can be attributed largely to an increase in latent heating.

To explain these patterns, we compute Hovmöller plots for the vertical wind, specific humidity and the vertical PV gradient (Fig. 9). The specific humidity and vertical PV gradient have little to no overlap, and can be used to separate the Hovmöller plane into two zones — the lower zone with moisture availability and the higher zone with a large gradient of PV. At the lower

https://doi.org/10.5194/egusphere-2026-4895
Preprint. Discussion started: 19 August 2026

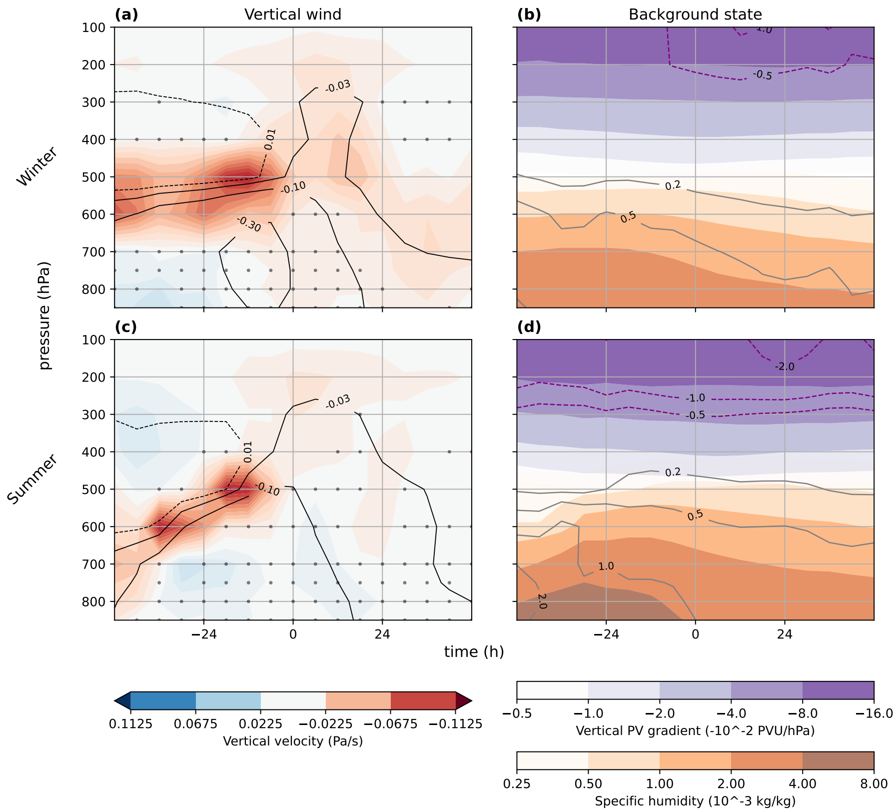

Figure 9. Difference Hovmöller plots for the vertical velocity between the control and p4K cyclones for the strongest winter (panel a) and summer (panel c) cyclones. The values of these quantities for the control run are overlaid as contours. The stippling shows regions where the magnitude of the difference between runs does not exceed 10 percent of its absolute value in the control run. Panels (b) and (d) show the Hovmöller plots for the specific humidity and vertical PV gradient (averaged over the cyclone mask). These quantities are shown in the same plots as they have almost no region of overlap. The difference (p4K minus control) is depicted by the contour lines — in grey for specific humidity and purple for the vertical PV gradient.

levels, the vertical wind does not change much with warming (less than 10 percent of its value in the control run, shown by the stippling). However, the specific humidity at these levels increases by about 20–30 percent for both seasons. This fact, combined with the larger vertical winds in winter cyclones, can qualitatively explain why these cyclones have a stronger low-level response to warming — the larger vertical winds in winter cyclones enables them to utilise the increase in low-level moisture more readily and produce a larger increase in latent heat release (not shown).

Shifting our focus from the low-levels to the vertical structure of the cyclones, we see that the vertical wind Hovmöller plots (panels a, c of Fig. 9) clearly depict the regions of ascent associated with the low-level cyclone and the descent due to dry intrusion from the upper levels. With warming, the strongest changes to vertical velocity occur at the boundary between the ascent and the descent. This can be explained by a decreased downward penetration of upper-level PV in the presence of

https://doi.org/10.5194/egusphere-2026-4895
Preprint. Discussion started: 19 August 2026

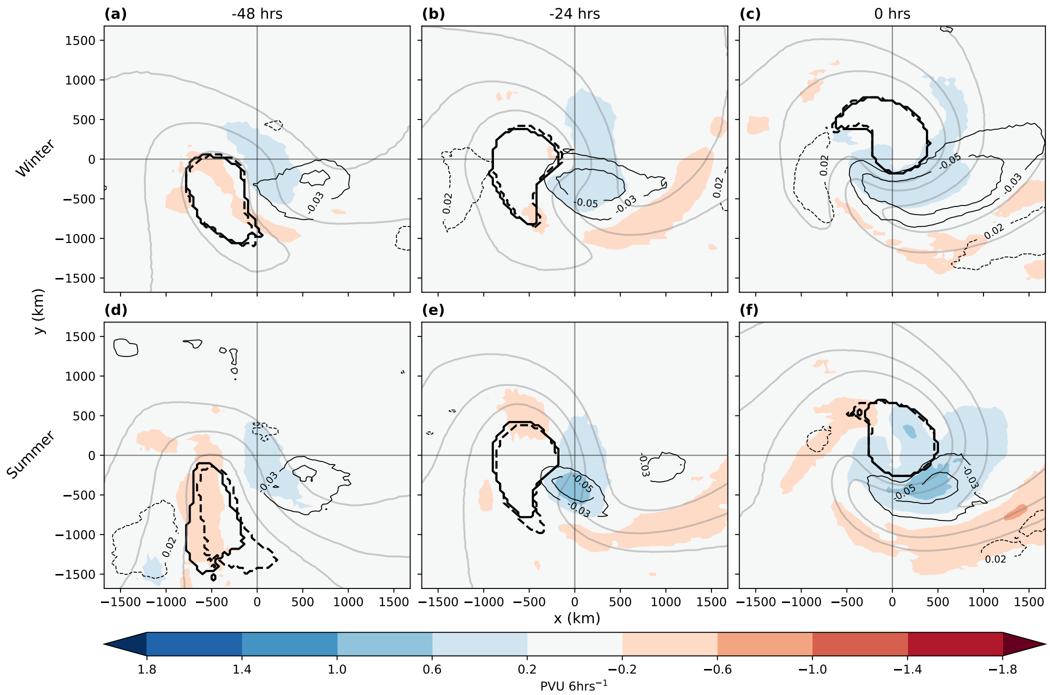

Figure 10. Cyclone-centric plots at 300 hPa for the difference in total PV tendency (p4K minus control) for the strongest winter and summer cyclones. The thick contour lines show the cyclone mask at 300 hPa, with the solid and dashed lines representing the cyclone for the p4K and control runs, respectively. The changes in vertical wind (in Pa/s) are shown by the thin contour lines. For reference, the grey contour lines in the background show the mean PV field at 300 hPa for values –1, –2 and –3 PVU.

increased diabatic tendencies, and is a typical characteristic of strong diabatic heating in cyclones (Ahmadi-Givi et al., 2004). The increase in vertical velocity with warming extends into the upper troposphere close to the time of cyclone maximum, consistent with previous studies that show that the inclusion of diabatic processes leads to stronger vertical velocities in cyclones (e.g. Kuo et al., 1991). This increase in vertical velocities occurs in the zone of large vertical PV gradient, leading to more advection of low-PV air into the upper troposphere, resulting in the upper level PV decay patterns seen in Fig. 8.

Finally, to understand how the upper-level cyclone responds to warming, we examine the patterns of the total PV tendency changes at 300 hPa (Fig. 10). The cyclone masks at this level for the two runs are very similar and sample the same regions. The PV tendency changes at this level lead to an increased decay of cyclonic PV directly above the location of the warm conveyor belt. Although some of this is due to the direct effect of the diabatic term (not shown), the majority of this pattern is due to the indirect, adiabatic increase of vertical velocities advecting more low-PV air into this level, consistent with Methven (2015). This is substantiated by the increase in ascent being largely co-located with the PV decay in Fig. 10. The slight interactions of the PV tendencies and the cyclone mask lead to the upper level patterns of cyclonic PV decay seen in Fig. 8. This pattern

https://doi.org/10.5194/egusphere-2026-4895
Preprint. Discussion started: 19 August 2026

of increased PV decay on the equatorward flank of the upper-tropospheric jet stream, close to the location of the low-level cyclone, sharpens the horizontal PV gradients, in agreement with Harvey et al. (2020).

10 Conclusions

In this study, we combine the PV framework with a cyclone mask methodology to quantify the strengthening of cyclones sampled from CAM4 model runs. This methodology improves on previous attempts at quantifying the diabatic contribution to cyclone intensification and achieves a good agreement between the predicted and diagnosed PV changes, while also having a stronger theoretical basis and being more generally applicable. We show that the generalised diabatic tendency, which also accounts for the first-order vertical advection response due to diabatic heating, resembles the total PV intensification of the cyclone at the lower levels. In both the control and p4K runs, the total PV generated in the low-level (700–850 hPa) cyclone during the two days leading up to cyclone maximum intensity can be attributed to this term. Moreover, the diabatic contribution to the total maximum vorticity increases with cyclone strength, with the vorticity of the strongest cyclones across seasons and model experiments linked directly to diabatic PV generation. These results also hold up reasonably well (with some exceptions) in 10 years (1995–2004) of MERRA2 reanalysis data.

With warming, winter cyclones exhibit larger increases in low-level PV generation in comparison to summer cyclones, with most of this increase due to the diabatic term. We can link this seasonal asymmetry in PV response to the stronger increase in winter cyclone relative vorticity with warming. Focusing on the strongest cyclones, we find that the low-level PV response is primarily due to an increase in the low-level moisture availability, increasing by about 6–7 percent per kelvin of warming in both summer and winter, in line with what we expect from the Clausius-Clapeyron equation (Held and Soden, 2006; Schneider et al., 2010). The asymmetric response in winter cyclones can then be attributed in part to the larger low-level vertical winds which allows them to better utilise this moisture increase. The other effects of increased diabatic forcing include a decrease in the downward penetration of upper-level PV and an enhancement of PV decay in the upper troposphere directly above the low-level cyclone, sharpening the horizontal gradients of PV.

The results in this study highlight the importance of diabatic processes in determining the strength of cyclones, especially for the strongest ones. This also implies that resolving diabatic processes better would lead to an improvement in the underestimation of the intensification of extreme cyclones commonly found in climate models, consistent with Schemm (2023). The differences in response to warming with cyclone strength and the stronger increase in cyclone strength in winter indicate a “strong gets stronger” response to warming, at least in CESM CAM4. If real, such a response would have important implications for the extreme weather impacts associated with global warming in storm-track regions. Future work can extend this analysis to other atmospheric and coupled models to investigate if these results are consistent across models.

Code availability. The code used for this study has not been publicised. However, it may be made available on reasonable request to the corresponding author.

https://doi.org/10.5194/egusphere-2026-4895
Preprint. Discussion started: 19 August 2026

Data availability. CAM4 is available at https://github.com/ESCOMP/CESM. For a description of the model, see Neale et al. (2010). For the MERRA2 reanalysis datasets used in this study, see Global Modeling And Assimilation Office and Pawson (2015a, b)

Appendix A: Applying the methodology to MERRA2 data

Fig. A1 shows the Hovmöller plots (as in Fig. 3) obtained when the methodology was applied to MERRA2 (Global Modeling And Assimilation Office and Pawson, 2015a, b) data for years 1995–2004. We only aim to validate the methodology for reanalysis data, and we do not have a similar comparison for the changes in a warmer climate presented in the second half of the paper. Although the data has a temporal resolution of 3 hours, for consistency, we downsampled to a resolution of 6 hours.

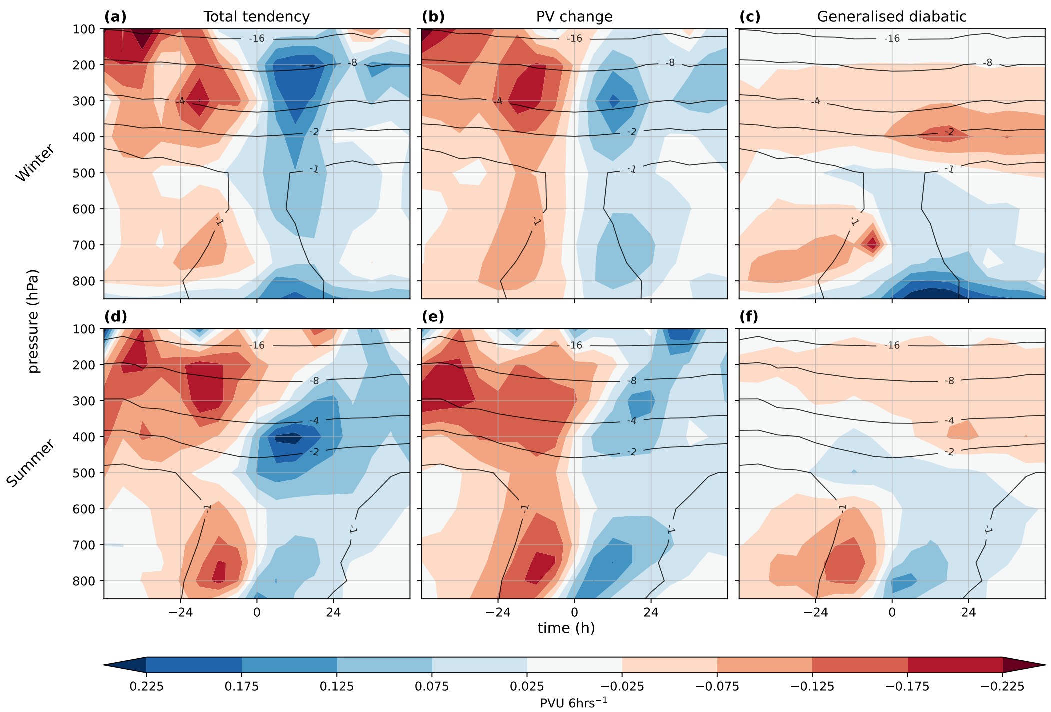

Figure A1. Hovmöller plots for the strongest summer and winter cyclones in MERRA2 data. (a),(d) The total PV intensification (as computed in Eq. 9). (b),(e) $d\langle Q\rangle/dt$, which should be similar to the total intensification. (c),(f) The generalised diabatic term (Eq. 5). The contour lines in all plots show the Hovmöller patterns for PV across time.

The results we obtain from MERRA2 are reasonably consistent to those from CAM4 (Figs. 3 and 4). However, the low-level diabatic tendency close to 850 hPa in winter is negative, leading to a mismatch between the total tendency and PV change.

Figure A2 presents the contributions of the diabatic and other processes to low-level PV and maximum vorticity (as in Figs. 5 and 6). Consistent with Fig. 5, the adiabatic term does not contribute much to the total PV tendency. The diabatic PV contributions are severely underestimated across most cyclone classes in winter, leading to a large mismatch between the PV

https://doi.org/10.5194/egusphere-2026-4895
Preprint. Discussion started: 19 August 2026

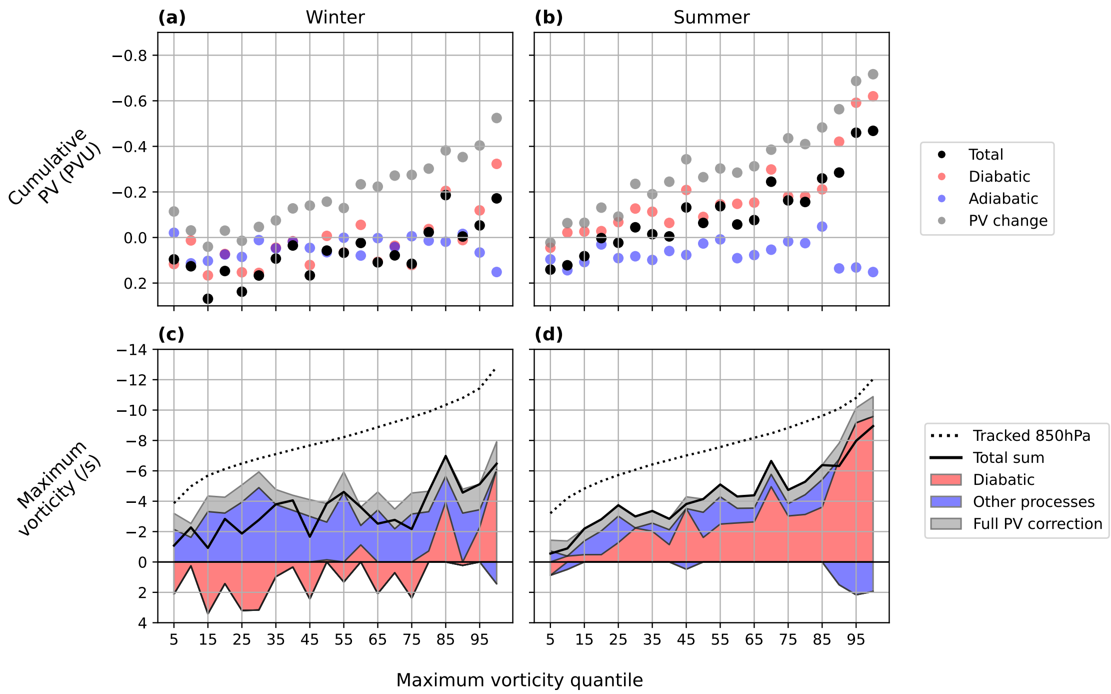

Figure A2. (a),(b) The total PV generated (computed using eq. 9) in cyclones of different strength groups in the two days preceding cyclone maximum vorticity. (c),(d) Contributions from the different processes to the total maximum vorticity of the average cyclone across strength classes.

change and total tendency. In summer, this contribution being better captured results in an increased agreement between the two. This pattern is consistent in the plots of vorticity contributions, where although predictability is retained, the underestimation of the diabatic term leads to a mismatch in the total vorticities.

Appendix B: Latent heating contribution

In Fig. B1, we compare the patterns of generalised diabatic tendencies we obtain from the total diabatic tendencies as opposed to only from latent heating, defined as the temperature tendency associated with phase changes of water, for example condensation or re-evaporation. We obtain similar low-level patterns irrespective of the choice of diabatic tendency term, both for CESM and MERRA2 data. However, the upper-level patterns associated with upper-tropospheric cooling are lost. There are also minor differences in the lowest levels, especially in winter, which is probably due to processes associated with the boundary layer.

https://doi.org/10.5194/egusphere-2026-4895
Preprint. Discussion started: 19 August 2026

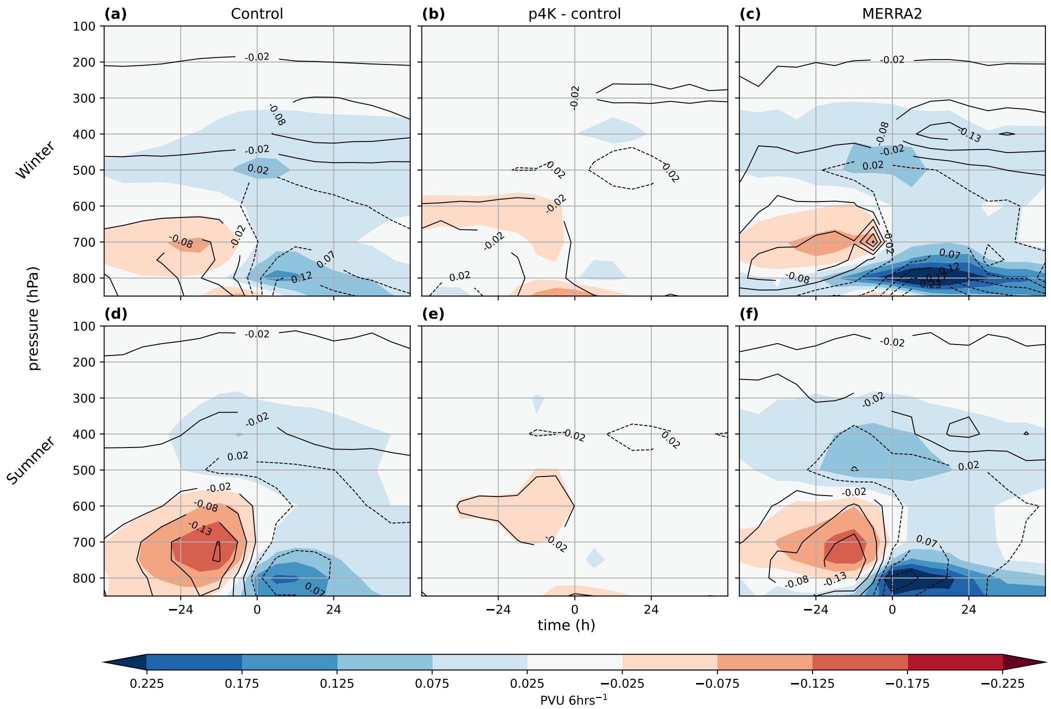

Figure B1. Comparison between the generalised diabatic Hovmöller patterns using the total diabatic tendency (shown as contour lines) and only diabatic tendencies due to latent heating (shown as filled contours).

Appendix C: Full PV correction

We can split Ertel PV (Q), the quantity of interest, into its three components as

$$Q = Q_x + Q_y + Q_z, \tag{C1}$$

where x and y are the horizontal directions and z along the vertical. Given that we are interested in the vorticity only along the vertical, we can rearrange the above equation to get

$$\xi_{\max} = \left(\frac{Q}{-g\frac{\partial \theta_{\max}}{\partial p}} - f_{\max} \right) + \frac{(Q_x + Q_y)}{g\frac{\partial \theta_{\max}}{\partial p}}. \tag{C2}$$

This equation is identical to Eq. 11, except for the last term on the RHS, which is the full PV correction term.

Author contributions. A.S. led the analysis and the writing of the manuscript. H.A. ran the model experiments. All authors contributed to the conceptualisation of the study and to the writing of the manuscript.

https://doi.org/10.5194/egusphere-2026-4895
Preprint. Discussion started: 19 August 2026

Competing interests. At least one of the (co-)authors is a member of the editorial board of Weather and Climate Dynamics.

Acknowledgements. A.S. and P.C. were supported by UK Research and Innovation (UKRI) under the UK government's Horizon Europe Funding Guarantee (grant EP/Y036123/1). A.S thanks Kevin Hodges for access and help with the tracking code and Paul O'Gorman, Sebastian Schemm and Koh Kawaguchi for productive discussions.

https://doi.org/10.5194/egusphere-2026-4895
Preprint. Discussion started: 19 August 2026

References

Ahmadi-Givi, F., Graig, G. C., and Plant, R. S.: The dynamics of a midlatitude cyclone with very strong latent-heat release, Quarterly Journal of the Royal Meteorological Society, 130, 295–323, https://doi.org/10.1256/qj.02.226, 2004.

Auestad, H., Shibu, A., Ceppi, P., and Woollings, T.: The Latent Heating Feedback on the Mid-Latitude Circulation, Geophysical Research Letters, 52, e2025GL116 437, https://doi.org/10.1029/2025GL116437, 2025.

Auestad, H., Shibu, A., Ceppi, P., and Woollings, T.: The latent heating feedback effect on storm tracks in current and future climates, npj Climate and Atmospheric Science, https://doi.org/10.1038/s41612-026-01421-9, 2026.

Booth, J. F., Wang, S., and Polvani, L.: Midlatitude storms in a moister world: lessons from idealized baroclinic life cycle experiments, Climate Dynamics, 41, 787–802, https://doi.org/10.1007/s00382-012-1472-3, 2013.

Büeler, D. and Pfahl, S.: Potential Vorticity Diagnostics to Quantify Effects of Latent Heating in Extratropical Cyclones. Part I: Methodology, Journal of the Atmospheric Sciences, https://doi.org/10.1175/JAS-D-17-0041.1, 2017.

Büeler, D. and Pfahl, S.: Potential Vorticity Diagnostics to Quantify Effects of Latent Heating in Extratropical Cyclones. Part II: Application to Idealized Climate Change Simulations, Journal of the Atmospheric Sciences, https://doi.org/10.1175/JAS-D-18-0342.1, 2019.

Catto, J. L. and Pfahl, S.: The importance of fronts for extreme precipitation, Journal of Geophysical Research: Atmospheres, 118, 10,791–10,801, https://doi.org/10.1002/jgrd.50852, 2013.

Chagnon, J. M. and Gray, S. L.: A Diabatically Generated Potential Vorticity Structure near the Extratropical Tropopause in Three Simulated Extratropical Cyclones, Monthly Weather Review, 143, 2337–2347, https://doi.org/10.1175/MWR-D-14-00092.1, 2015.

Chang, E. K. M., Lee, S., and Swanson, K. L.: Storm Track Dynamics, Journal of Climate, https://doi.org/10.1175/1520-0442(2002)015<02163:STD>2.0.CO;2, 2002.

Charney, J. G.: THE DYNAMICS OF LONG WAVES IN A BAROCLINIC WESTERLY CURRENT, Journal of the Atmospheric Sciences, https://doi.org/10.1175/1520-0469(1947)004<0136:TDOLWI>2.0.CO;2, 1947.

Davis, C. A. and Emanuel, K. A.: Potential Vorticity Diagnostics of Cyclogenesis, Monthly Weather Review, 119, 1929–1953, https://doi.org/10.1175/1520-0493(1991)119<1929:PVDOC>2.0.CO;2, 1991.

Davis, C. A., Stoelinga, M. T., and Kuo, Y.-H.: The Integrated Effect of Condensation in Numerical Simulations of Extratropical Cyclogenesis, Monthly Weather Review, https://doi.org/10.1175/1520-0493(1993)121<2309:TIEOCI>2.0.CO;2, 1993.

Eady, E. T.: Long Waves and Cyclone Waves, Tellus, 1, 33–52, https://doi.org/10.1111/j.2153-3490.1949.tb01265.x, 1949.

Emanuel, K. A., Fantini, M., and Thorpe, A. J.: Baroclinic Instability in an Environment of Small Stability to Slantwise Moist Convection. Part I: Two-Dimensional Models, Journal of the Atmospheric Sciences, 44, 1559–1573, https://doi.org/10.1175/1520-0469(1987)044<1559:BIIAEO>2.0.CO;2, 1987.

Global Modeling And Assimilation Office and Pawson, S.: MERRA-2 inst3_3d_asm_Np: 3d,3-Hourly,Instantaneous,Pressure-Level,Assimilation,Assimilated Meteorological Fields V5.12.4, https://doi.org/10.5067/QBZ6MG944HW0, 2015a.

Global Modeling And Assimilation Office and Pawson, S.: MERRA-2 tavg3_3d_tdt_Np: 3d,3-Hourly,Time-Averaged,Pressure-Level,Assimilation,Temperature Tendencies V5.12.4, https://doi.org/10.5067/9NCR9DDDOPFI, 2015b.

Gray, S. L., Volonté, A., Martínez-Alvarado, O., and Harvey, B. J.: A global climatology of sting-jet extratropical cyclones, Weather and Climate Dynamics, 5, 1523–1544, https://doi.org/10.5194/wcd-5-1523-2024, 2024.

Hartmann, D. L.: The Atmospheric General Circulation and Its Variability, Journal of the Meteorological Society of Japan. Ser. II, 85B, 123–143, https://doi.org/10.2151/jmsj.85B.123, 2007.

https://doi.org/10.5194/egusphere-2026-4895
Preprint. Discussion started: 19 August 2026

Harvey, B., Methven, J., Sanchez, C., and Schäfler, A.: Diabatic generation of negative potential vorticity and its impact on the North Atlantic jet stream, Quarterly Journal of the Royal Meteorological Society, 146, 1477–1497, https://doi.org/10.1002/qj.3747, 2020.

Hawcroft, M. K., Shaffrey, L. C., Hodges, K. I., and Dacre, H. F.: How much Northern Hemisphere precipitation is associated with extratropical cyclones?, Geophysical Research Letters, 39, https://doi.org/10.1029/2012GL053866, 2012.

Haynes, P. H. and McIntyre, M. E.: On the Evolution of Vorticity and Potential Vorticity in the Presence of Diabatic Heating and Frictional or Other Forces, Journal of the Atmospheric Sciences, 44, 828–841, https://doi.org/10.1175/1520-0469(1987)044<0828:OTEOVA>2.0.CO;2, 1987.

Held, I. M. and Soden, B. J.: Robust Responses of the Hydrological Cycle to Global Warming, Journal of Climate, https://doi.org/10.1175/JCLI3990.1, 2006.

Hodges, K. I.: A General Method for Tracking Analysis and Its Application to Meteorological Data, Monthly Weather Review, https://doi.org/10.1175/1520-0493(1994)122<2573:AGMFTA>2.0.CO;2, 1994.

Hodges, K. I.: Feature Tracking on the Unit Sphere, Monthly Weather Review, https://doi.org/10.1175/1520-0493(1995)123<3458:FTOTUS>2.0.CO;2, 1995.

Hodges, K. I.: Adaptive Constraints for Feature Tracking, Monthly Weather Review, https://doi.org/10.1175/1520-0493(1999)127<1362:ACFFT>2.0.CO;2, 1999.

Hoskins, B. J. and Valdes, P. J.: On the Existence of Storm-Tracks, Journal of the Atmospheric Sciences, https://journals.ametsoc.org/view/journals/atsc/47/15/1520-0469_1990_047_1854_oteost_2_0_co_2.xml, 1990.

Hoskins, B. J., McIntyre, M. E., and Robertson, A. W.: On the use and significance of isentropic potential vorticity maps, Quarterly Journal of the Royal Meteorological Society, 111, 877–946, https://doi.org/10.1002/qj.49711147002, 1985.

Hurrell, J. W., Hack, J. J., Shea, D., Caron, J. M., and Rosinski, J.: A New Sea Surface Temperature and Sea Ice Boundary Dataset for the Community Atmosphere Model, Journal of Climate, https://doi.org/10.1175/2008JCLI2292.1, 2008.

Kohl, M. and O'Gorman, P. A.: The Diabatic Rossby Vortex: Growth Rate, Length Scale, and the Wave–Vortex Transition, Journal of the Atmospheric Sciences, https://doi.org/10.1175/JAS-D-22-0022.1, 2022.

Konstali, K., Spensberger, C., Spengler, T., and Sorteberg, A.: Global Attribution of Precipitation to Weather Features, Journal of Climate, https://doi.org/10.1175/JCLI-D-23-0293.1, 2024.

Kuo, Y.-H., Shapiro, M. A., and Donall, E. G.: The Interaction between Baroclinic and Diabatic Processes in a Numerical Simulation of a Rapidly Intensifying Extratropical Marine Cyclone, Monthly Weather Review, 119, 368–384, https://doi.org/10.1175/1520-0493(1991)119<0368:TIBBAD>2.0.CO;2, 1991.

Köhler, D. and Sinclair, V. A.: Differentiating Average and Extreme Extra-Tropical Cyclones by Their Vertical Tilt and Potential Vorticity Structure, Geophysical Research Letters, 53, e2025GL119 822, https://doi.org/10.1029/2025GL119822, 2026.

Martínez-Alvarado, O., Gray, S. L., and Methven, J.: Diabatic Processes and the Evolution of Two Contrasting Summer Extratropical Cyclones, Monthly Weather Review, 144, 3251–3276, https://doi.org/10.1175/MWR-D-15-0395.1, 2016.

Methven, J.: Potential vorticity in warm conveyor belt outflow, Quarterly Journal of the Royal Meteorological Society, 141, 1065–1071, https://doi.org/10.1002/qj.2393, 2015.

Neale, A. R., Richter, A. J. H., Conley, A. A. J., Park, A. S., Lauritzen, A. P. H., Gettelman, A. A., Williamson, A. D., Rasch, A. P. J., Vavrus, A. S. J., Taylor, A. M. A., Collins, A. W., Zhang, A. M., and Lin, A. S.: Description of the NCAR Community Atmosphere Model (CAM 4.0), 2010.

https://doi.org/10.5194/egusphere-2026-4895
Preprint. Discussion started: 19 August 2026

Owen, L. E., Catto, J. L., Stephenson, D. B., and Dunstone, N. J.: Compound precipitation and wind extremes over Europe and their relationship to extratropical cyclones, Weather and Climate Extremes, 33, 100 342, https://doi.org/10.1016/j.wace.2021.100342, 2021.

Pfahl, S., O'Gorman, P. A., and Singh, M. S.: Extratropical Cyclones in Idealized Simulations of Changed Climates, Journal of Climate, https://doi.org/10.1175/JCLI-D-14-00816.1, 2015.

Priestley, M. D. K. and Catto, J. L.: Future changes in the extratropical storm tracks and cyclone intensity, wind speed, and structure, Weather and Climate Dynamics, 3, 337–360, https://doi.org/10.5194/wcd-3-337-2022, 2022.

Priestley, M. D. K., Ackerley, D., Catto, J. L., Hodges, K. I., McDonald, R. E., and Lee, R. W.: An Overview of the Extratropical Storm Tracks in CMIP6 Historical Simulations, Journal of Climate, https://doi.org/10.1175/JCLI-D-19-0928.1, 2020.

Schemm, S.: Toward Eliminating the Decades-Old "Too Zonal and Too Equatorward" Storm-Track Bias in Climate Models, Journal of Advances in Modeling Earth Systems, 15, e2022MS003 482, https://doi.org/10.1029/2022MS003482, 2023.

Schneider, T., O'Gorman, P. A., and Levine, X. J.: Water Vapor and the Dynamics of Climate Changes, Reviews of Geophysics, 48, https://doi.org/10.1029/2009RG000302, 2010.

Sinclair, V. A., Rantanen, M., Haapanala, P., Räisänen, J., and Järvinen, H.: The characteristics and structure of extra-tropical cyclones in a warmer climate, Weather and Climate Dynamics, 1, 1–25, https://doi.org/10.5194/wcd-1-1-2020, 2020.

Stoelinga, M. T.: A Potential Vorticity-Based Study of the Role of Diabatic Heating and Friction in a Numerically Simulated Baroclinic Cyclone, Monthly Weather Review, https://doi.org/10.1175/1520-0493(1996)124<0849:APVBSO>2.0.CO;2, 1996.

Tamarin, T. and Kaspi, Y.: The Poleward Motion of Extratropical Cyclones from a Potential Vorticity Tendency Analysis, Journal of the Atmospheric Sciences, https://doi.org/10.1175/JAS-D-15-0168.1, 2016.

Tamarin-Brodsky, T. and Kaspi, Y.: Enhanced poleward propagation of storms under climate change, Nature Geoscience, 10, 908–913, https://doi.org/10.1038/s41561-017-0001-8, 2017.

Tierney, G., Posselt, D. J., and Booth, J. F.: An examination of extratropical cyclone response to changes in baroclinicity and temperature in an idealized environment, Climate Dynamics, 51, 3829–3846, https://doi.org/10.1007/s00382-018-4115-5, 2018.

Čampa, J. and Wernli, H.: A PV Perspective on the Vertical Structure of Mature Midlatitude Cyclones in the Northern Hemisphere, Journal of the Atmospheric Sciences, https://doi.org/10.1175/JAS-D-11-050.1, 2012.